Optics Letters

Soliton repetition rate in a silicon-nitride microresonator

Chengying Bao,[1,*] Yi Xuan,[1,2] Cong Wang,[1] Jose A. Jaramillo-Villegas,[1,3] Daniel E. Leaird,[1] Minghao Qi,[1,2] and Andrew M. Weiner[1,2]

[1]School of Electrical and Computer Engineering, Purdue University, 465 Northwestern Avenue, West Lafayette, Indiana 47907-2035, USA
[2]Birck Nanotechnology Center, Purdue University, 1205 West State Street, West Lafayette, Indiana 47907, USA
[3]Facultad de Ingenierías, Universidad Tecnológica de Pereira, Pereira, Risaralda 66003, Colombia
*Corresponding author: bao33@purdue.edu

Received 15 November 2016; revised 3 January 2017; accepted 19 January 2017; posted 23 January 2017 (Doc. ID 280577); published 9 February 2017

The repetition rate of a Kerr comb composed of a single soliton in an anomalous group velocity dispersion silicon-nitride microcavity is measured as a function of pump frequency. By comparing operation in the soliton and non-soliton states, the contributions from the Raman soliton self-frequency shift (SSFS) and the thermal effects are evaluated; the SSFS is found to dominate the changes in the repetition rate, similar to silica cavities. The relationship between the changes in the repetition rate and the pump frequency detuning is found to be independent of the nonlinearity coefficient and dispersion of the cavity. Modeling of the repetition rate change by using the generalized Lugiato–Lefever equation is discussed; the Kerr shock is found to have only a minor effect on repetition rate for cavity solitons with duration down to ~50 fs.

OCIS codes: (190.5530) Pulse propagation and temporal solitons; (190.4390) Nonlinear optics, integrated optics.

https://doi.org/10.1364/OL.42.000759

Optical frequency combs consist of a series of discrete, evenly spaced spectral lines, whose frequency is $\nu_n = nf_r + f_0$, where f_r is the repetition rate and f_0 is the carrier envelope offset frequency [1]. Microresonator-based Kerr combs [2] show potential as a compact replacement for conventional mode-locked laser combs, but they generally do not reach similar stability. Since the integer n is generally large, the frequency of an individual comb line is extremely sensitive to the fluctuation of f_r. Hence, investigating the repetition rate of Kerr combs is important to the improvement of Kerr combs. Thermal effects and mechanical stretching have been exploited to stabilize the f_r of the Kerr combs [3–6]. Recently, cavity solitons (CSs) have been demonstrated in microresonators [7–11]. Unlike other non-soliton coherent operation regimes, CSs exhibit a soliton self-frequency shift (SSFS) induced by stimulated Raman scattering (SRS) [9–14]. The center frequency shift arising through a SSFS can affect f_r via dispersion, constituting a new mechanism for changes in the repetition rate. The SSFS has been shown to be the main reason of the repetition rate change in a 22 GHz silica microcavity [13]. In addition to silica, silicon-nitride (SiN) is an important platform for integrated soliton Kerr comb generation. Considering the difference of thermal effects and Raman effect between silica and SiN, it is important to compare the relative importance of the SSFS and thermal contributions to soliton repetition rate changes (denoted Δf_r) in SiN microresonators. In this Letter, we use frequency comb-assisted-laser diode spectroscopy [15,16] to measure the Δf_r for a 227 GHz soliton Kerr comb generated from a SiN microresonator. We find that f_r can vary ~25 MHz as the pump frequency is tuned, while maintaining the single soliton state. The contributions from the SSFS and thermal effects are isolated and compared, and the SSFS is found to dominate.

The Lugiato–Lefever equation (LLE) is now widely used to model Kerr combs [17,18]. However, it has rarely been used for the modeling of changes in repetition rate and pulse timing. Whether the LLE is capable of capturing such changes is an interesting question, since pulse propagation is averaged in the derivation of LLE. Changes in pulse timing have been modeled and compared to the experiment quite recently in the normal dispersion regime [19]. Here, we further show LLE is capable of modeling of the changes in f_r that we observe in experiments in the CS regime. Simulations of pulse timing based on LLE also give insights into the influence of Kerr shock, and we show that the Kerr shock has a minor effect on f_r for pulses as short as 50 fs.

For mode-locked lasers, the center frequency is constrained by the net gain spectrum; a weak modulation of the pump power can only change the center frequency slightly by several tens of gigahertz [20,21]. Hence, this center frequency shift will not change f_r significantly. Unlike mode-locked lasers and non-soliton coherent regimes of Kerr combs, the center frequency of CSs is strongly influenced by the interaction with the waveguide via SRS [12]. Tuning the pump frequency can vary this SSFS over several terahertz [12], thus affecting f_r strongly. Here, we measure the dependence of f_r on the SSFS via tuning the pump frequency within the single CS regime.

We study a SiN microresonator with a 100 μm ring radius, 800 × 2000 nm waveguide geometry, and a loaded Q-factor of 2.4×10^6, with which we are able to generate a Kerr comb

composed of single-cavity solitons at a 227 GHz repetition rate, when pumping at the resonance around 1551.3 nm. The device has a drop port (with a power coupling coefficient of 1.6×10^{-4}) [10], which allows convenient measurement of the intracavity power without the directly transmitted pump that is present at the through port. Frequency-comb-assisted laser diode spectroscopy is used to measure the line spacing of the generated comb [15,16]. A cw diode laser is used to sweep across the Kerr comb, generating beat notes that are recorded by an oscilloscope after bandpass filtering. A femtosecond frequency comb is used for calibration of the laser frequency sweep. This method has been shown to have megahertz resolution and accuracy similar to that achieved using the electro-optic modulation-assisted measurement of the line spacing [15,16].

As an example, the relative frequencies for different comb lines are shown in Fig. 1(a). When we zoom into a single line in the CS regime, we can see two narrow peaks, since the cw laser generates a beat note that can pass the bandpass filter when it is both to the red and to the blue of the comb line [inset (i) in Fig. 1]. In contrast, if the Kerr comb is in the chaotic regime (pumped at a shorter wavelength), the beat with the cw laser is broad and structured [inset (ii) in Fig. 1(a)]. We can fit the measured relative frequencies of the Kerr comb lines to a line to get f_r [inset of Fig. 1(b)]. The power and SSFS of the CS will also change when we tune the pump frequency [7,12]. For our device, the single CS can be maintained over a 1.1 GHz range of pump frequency; f_r changes by ~25 MHz in this range, with a slope of 22.0 MHz/GHz [Fig. 1(b)]. Note that this slope for a 18 GHz SiN microresonator-based Kerr comb was measured to be 57 kHz/GHz for a non-soliton state in [5].

We also measure the spectrum of the generated CS, which fits well to a sech^2 function, except some spikes from the mode interaction [Fig. 1(c)] [22]. The spikes can lead to spectral recoiling [23]. This recoiling is relatively weak in our device, as the spikes have moderate intensity and are located both to the red and to the blue of the spectral center. The fit gives the

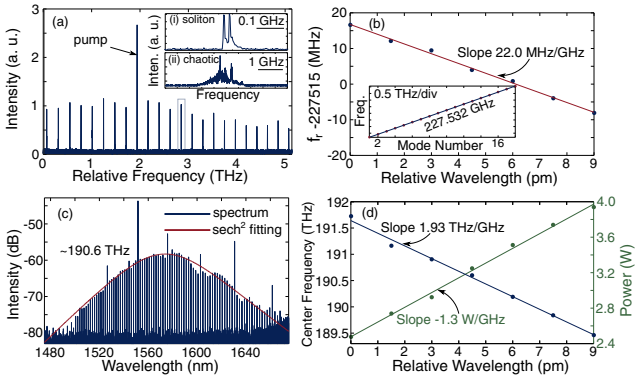

Fig. 1. (a) Frequency markers from the beat between the Kerr comb and the sweeping cw laser. Inset (i) shows the zoom in a single frequency marker in the shaded box in the soliton state, while inset (ii) shows the frequency marker in the chaotic state. The frequency axis is calibrated by the frequency markers beating with the femtosecond frequency comb. (b) Dependence of f_r on the pump wavelength; the inset shows a typical linear fitting of the Kerr comb frequency markers to get f_r. (c) Soliton spectrum from the drop port and its sech^2 fit. (d) Measured dependence of the center frequency shift (blue dots) and the intracavity power (green dots) on the pump wavelength and their corresponding linear fits.

center frequency of the CS. When the pump frequency varies, the center frequency of the CS also changes nearly linearly with the pump frequency [12] [Fig. 1(d)], having a slope of 1.93 THz/GHz. Using the drop port, we are also able to measure the average intracavity power; the power decreases nearly linearly with the pump frequency (increases with pump wavelength and detuning), with a slope of –1.3 W/GHz.

The measurement of the SSFS and intracavity power allows comparison between the influence of the SSFS and thermal effects on Δf_r. The SSFS contribution to the repetition rate change, denoted Δf_r^s, can be calculated as

$$\Delta f_r^s = \Delta\left(\frac{1}{\beta_1 L}\right) = -\frac{L\Delta\beta_1}{(\beta_1 L)^2} = -Lf_r^2\beta_2\Delta\Omega_{cs}, \quad (1)$$

where L is the length of the cavity, $1/\beta_1$ is the group velocity, β_2 is the group velocity dispersion, and Ω_{cs} is the SSFS in angular frequency. The spectral recoil from the mode interaction in a MgF_2 cavity affects f_r in a similar way [23]. From Eq. (1), we can see that Δf_r^s depends on dispersion of the cavity for a given SSFS. To check this relation, we measure the dispersion using frequency-comb-assisted spectroscopy [15]. We show the deviation of the resonance from the equidistant spacing, $d_{\text{int}} = \nu_\mu - \nu_0 - \mu d_1 \approx d_2\mu^2/2$ (ν_μ is the resonant frequency of mode μ, d_1 is the free spectral range, and d_2 is the dispersion coefficient), in Fig. 2(a). From a quadratic fit, d_2 is found to be 3.1 MHz, equivalent to $\beta_2 = -66$ ps^2/km [24], close to the simulated dispersion of –51 ps^2/km [10].

If we assume Δf_r in Fig. 1(b) is driven solely by the SSFS, we can extract β_2 by using Eq. (1). For an on-chip pump power of 800 mW, we obtain β_2 is –55 ps^2/km. Furthermore, the obtained value remains nearly the same under different pump powers [Fig. 2(b)]. The small fluctuation (55 ± 2.8 ps^2/km) is because of the measurement uncertainty. More importantly, these values are quite close to those obtained via waveguide simulations and linear spectroscopy measurements. This agreement suggests that the change in repetition rate is dominated by the SSFS.

Furthermore, the SSFS (Ω_{cs}) can be approximated as [24]

$$\Omega_{cs} = \frac{8c\tau_R Q}{15n_g\omega_r}\frac{\beta_2}{\tau_s^4} = \frac{8\tau_R Q}{15\omega_r}\frac{\beta_2}{\beta_1\tau_s^4}, \quad (2)$$

where ω_r, τ_R, n_g, c, Q, and τ_s are the resonance frequency of the cavity, Raman time constant, effective group index, speed of

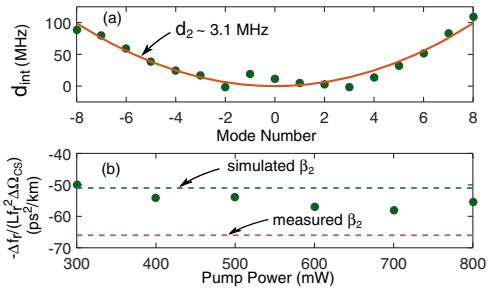

Fig. 2. (a) Resonance deviation from even spacing (circles) measured using frequency-comb-assisted spectroscopy and quadratic fit (line), yielding a dispersion of –66 ps^2/km. (b) Dispersion (circles) extracted from Eq. (1), based on the measurements of the SSFS and Δf_r at different pump powers, assuming that the observed changes in repetition rate arise from the SSFS only. These values are in close agreement with the dispersion measured using comb-assisted spectroscopy and computed via waveguide simulations.

light, quality factor, and pulse width of the CS, respectively. The peak power (P_0) of CSs follows the soliton law, $\gamma P_0 = |\beta_2|/\tau_s^2$ (γ is the nonlinear coefficient); P_0 also scales nearly linearly with pump frequency detuning [9,25],

$$\gamma P_0 \approx \frac{2(\omega_r - \omega_p)t_R}{L} \approx 2(\omega_r - \omega_p)\beta_1, \quad (3)$$

where ω_p is the pump frequency, and t_R is the round-trip time. Based on Eqs. (2) and (3), the SSFS depends quadratically on pump frequency detuning. The nearly linear dependence in Fig. 1(d) arises because the detuning varies by only ±33%, compared to its mean value over the tuning range. (The bandwidth of the spectrum changes within 5.2–7.3 THz in Fig. 1; the detuning change can be estimated based on Eq. (3) and the soliton law.) Combining Eqs. (1)–(3) and defining the pump frequency detuning as $\omega_d = \omega_r - \omega_p$, we can get

$$\Delta f_r^s \approx -\frac{32\tau_R}{15}\frac{f_r Q}{\omega_r}\Delta\omega_d^2 \approx -\frac{64\tau_R}{15}\frac{\omega_d Q}{\omega_r} f_r \Delta\omega_d. \quad (4)$$

This relationship means $\Delta f_r^s/\Delta\omega_d$ is not directly dependent on the dispersion or nonlinear coefficient of the cavity.

We now assess the contribution of the thermo-optic (TO) effect to the change in repetition rate, which we denote Δf_r^t. This contribution can be expressed as

$$\Delta f_r^t = \Delta\left(\frac{c}{n_g L}\right) = -\frac{L}{c}\left(\frac{c^2}{n_g^2 L^2}\right)\Delta n_g = -\frac{L f_r^2}{c}\Delta n_g, \quad (5)$$

where Δn_g is the change of the group index due to the TO effect. Δn_g can be written as

$$\Delta n_g = \frac{dn_g}{dT}\frac{\tau_\theta(\alpha f_\theta)\Delta P}{C_\theta \rho A_{\text{eff}}}. \quad (6)$$

Here, dn_g/dT is the derivative of the effective group index with respect to temperature. To get a value for dn_g/dT, we perform waveguide simulations to obtain the effective phase index (n_p) of the microresonator for different wavelengths and temperatures; the group index is $n_g = n_p - \lambda dn_p/d\lambda$ [16]. Using the same TO coefficient for SiN and SiO_2 as [16], we find $dn_g/dT = 3.2 \times 10^{-5}$ K^{-1}. $C_\theta = 760$ J/(kg · K) is the heat capacity of SiN, $\rho = 2.2 \times 10^3$ kg/m^3 is the density of SiN [26], the time constant (τ_θ) was measured to be 0.25 μs in a similar microresonator in our group's previous work [27], α is the propagation loss coefficient (measured to be $1.7 \times 10^{-3}/628$ μm^{-1}), f_θ is the fraction of the absorbed energy that is converted to heat, A_{eff} is the effective mode area (extracted to be 0.67 μm^2 from the simulation based on the geometry of the ring), and ΔP is the change of average intracavity power. Note that we neglect thermal expansion in the calculation; however, the SiN ring is embedded in a 4 μm thick SiO_2 layer, and the expansion should be small [16]. To get the upper bound estimate of Δf_r^t, we set $f_\theta = 1$. Based on Eqs. (5) and (6), the thermal-induced Δf_r^t is 3.1 MHz for a measured intracavity power change of 1.5 W. Even though $f_\theta = 1$ overestimates the contribution from the TO effect, the estimated value for Δf_r^t is still an order of magnitude smaller than the observed 25 MHz change in comb spacing, suggesting that the contribution from the TO effect is much weaker than that of the SSFS.

To further isolate the thermal contribution, we conduct another measurement of Δf_r in a stable modulation instability regime [see the inset of Fig. 3(b) for a typical spectrum]. Our measurements show that, in this state, changes in the center frequency of the comb are very small within the range

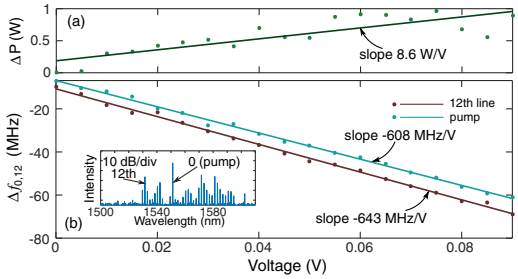

Fig. 3. (a) Measured intracavity power change and its linear fit versus the voltage to control the piezo of the pump laser. (b) Measured frequency change and the linear fit for the pump line and the 12th comb line versus the piezo voltage. The change of the frequency for the 12th comb line is shifted from zero for clarity. The inset shows the spectrum of the stable modulation instability state.

over which the laser is tuned. The pump line and the 12th line are filtered by a pulse shaper to beat with the femtosecond comb, thus measuring $12\Delta f_r$. We record both the change of the frequencies of these two Kerr comb lines and the average comb power with respect to the voltage used to control the piezo of the external cavity diode pump laser in Fig. 3. Both the frequencies and the comb power are found to change nearly linearly. From the linear fits, we find that the coefficient of the repetition rate change with intracavity power is −0.3 MHz/W. Hence, for the measured 1.5 W change in the intracavity power in Fig. 1(d), the contribution to Δf_r is only 0.45 MHz, which is much smaller than the change in the repetition rate observed.

Since Δf_r is dominated by the SSFS, which can be modeled by the generalized LLE [9,12,24], we perform simulations using the generalized LLE to look into the pulse timing dynamics. We write the generalized LLE [12,18,22,28] as

$$\left(t_R\frac{\partial}{\partial t} + \frac{\kappa_0+\kappa_1}{2} + i\delta_0 + i\frac{\beta_2 L}{2}\frac{\partial^2}{\partial\tau^2}\right)E - \sqrt{\kappa_1}E_{in} - i\gamma L\left(1 + \frac{i}{\omega_0}\frac{\partial}{\partial\tau}\right)\left(E\int_{-\infty}^{+\infty} R(\tau')|E(t,\tau-\tau')|^2 d\tau'\right) = 0, \quad (7)$$

where κ_0, κ_1, and E_{in} are the intrinsic loss, external coupling coefficient, and pump field at the frequency ω_0, respectively. $R(\tau) = (1-\Theta_R)\delta(\tau) + \Theta_R h_R(\tau)$ is the nonlinear response, including both the electronic and the delayed Raman response ($h_R(\tau)$). The Raman effect is calculated in the frequency domain with a Lorentzian gain spectrum (centered at −14.3 THz with a bandwidth of 2.1 THz) with the Raman fraction Θ_R chosen as 0.13 [22,29]. High-order dispersion is omitted, since it has a minor effect for the studied device [22].

Here, we show the simulation results for a typical CS generated at 305 mW pump power and detuning $\delta_0 = 0.0303$ in a SiN microresonator with $\gamma = 0.9$ (W · m)$^{-1}$, $\beta_2 = -66$ ps^2/km, $\kappa_0 = 0.002$, and $\kappa_1 = 0.0004$. The spectrum of the CS is shown in Fig. 4(a), corresponding to a pulse width $\tau_s = 50$ fs. The shift between the center frequency of the spectrum and the pump frequency, i.e., the SSFS, is $-2\pi \times 2.65$ THz, which matches the measured SSFS in Fig. 1(d). According to Eq. (1), this leads to a change of the repetition rate of −35.6 MHz for $f_r = 227$ GHz. To compare this value with the pulse timing dynamics in the LLE simulation, we show the temporal-spatial dynamics of the simulated CS in Fig. 4(b). Due to the SSFS, the peak of the CS envelope experiences additional delay with a slope of

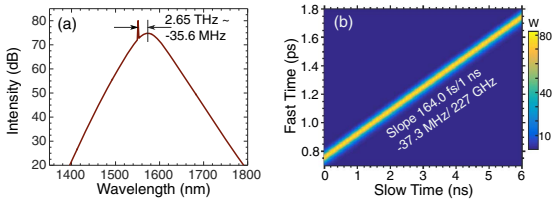

Fig. 4. (a) Simulated spectrum of the intracavity CS, showing a SSFS of $-2\pi \times 2.65$ THz. (b) Temporal evolution of the CS train on slow time. The peak of the temporal evolution trace has a slope of 164 fs/1 ns.

164.0 fs/ns; without the SSFS, the plot would appear as a horizontal line. From the relationship $-\Delta t_R/t_R = \Delta f_r/f_r$, this slope is equivalent to $\Delta f_r = -37.2$ MHz, in close agreement with the SSFS predicted −35.6 MHz. This supports the notion that pulse timing information is retained in the LLE, despite the inherent averaging in the derivation.

The slight difference in the two values of Δf_r can be attributed to the inclusion of the Kerr shock (KS) in the simulation, which affects the group velocity of the CS [20,21,25,30]. The difference in the simulated and the SSFS predicted Δf_r is equivalent to a change of round-trip time of $\Delta t_R/t_R = 7.2$ fs/ns. Since the change of group velocity (v_g) for sech-soliton induced by the KS is $\Delta(1/v_g) \approx \gamma P_0/\omega_0$ [30], the variation of the round-trip time induced by the KS yields

$$\frac{\Delta t_R}{t_R} = \frac{\Delta(L/v_g)}{t_R} = \Delta\left(\frac{1}{v_g}\right)\frac{L}{t_R} \approx \frac{\gamma P_0 L}{\omega_0 t_R}. \tag{8}$$

Based on Eq. (8), $\Delta t_R/t_R$ induced by the KS is 8.8 fs/ns, which is close to the simulated 7.2 fs/ns. The residual discrepancy may result from the deviation of the simulated CS from the sech-pulse. Furthermore, when excluding the KS in the simulation, the SSFS increases slightly to $-2\pi \times 2.73$ THz. The round-trip time change predicted from this SSFS is $\Delta t_R/t_R = 161.6$ fs/ns based on Eq. (1). On the other hand, if we extract the timing of the CS envelope peak from the simulation without the KS, we find a slope of 161.7 fs/ns, in excellent agreement with the SSFS prediction. Hence, the generalized LLE can be used to model pulse timing and changes in the repetition rate induced both by the SSFS and the KS.

Since the pulse dynamics in nonlinear resonators strongly affect the comb performance [20,21,31], an accurate theoretical model to investigate the intracavity pulse dynamics is important to the optimization of frequency combs. For mode-locked lasers, the complex Ginzburg–Landau equation is usually used to model the pulse dynamics [32]. However, effects such as gain relaxation, spectral filtering, and the resulting mode-locking state, are usually hard to model accurately. For CSs in passive microresonators, the absence of active gain and nonlinear absorption makes it feasible to model the pulse timing dynamics accurately. If noise sources are added to the model correctly, we can expect a full characterization of the pulse dynamics.

In summary, the SSFS induces a considerable change in the soliton repetition rate from a SiN microresonator. Both experimental and modeling results suggest that the SSFS can lead to changes in the repetition rate much larger than those caused by the thermo-optic effect. The SSFS provides a useful degree of freedom to broaden the locking range of repetition. KS is found to have a minor effect on soliton timing for a pulse as short as ~50 fs. Understanding the pulse dynamics and the noise behavior of the soliton Kerr combs based on the LLE can be valuable for the improvement of Kerr comb stability.

Funding. Air Force Office of Scientific Research (AFOSR) (FA9550-15-1-0211); Defense Advanced Research Projects Agency (DARPA) (W31P40-13-1-0018); National Science Foundation (NSF) (ECCS-1509578).

REFERENCES

1. S. T. Cundiff and J. Ye, Rev. Mod. Phys. **75**, 325 (2003).
2. T. J. Kippenberg, R. Holzwarth, and S. Diddams, Science **332**, 555 (2011).
3. P. Del'Haye, O. Arcizet, A. Schliesser, R. Holzwarth, and T. J. Kippenberg, Phys. Rev. Lett. **101**, 053903 (2008).
4. S. B. Papp, P. Del'Haye, and S. A. Diddams, Phys. Rev. X **3**, 031003 (2013).
5. S.-W. Huang, J. Yang, J. Lim, H. Zhou, M. Yu, D.-L. Kwong, and C. Wong, Sci. Rep. **5**, 13355 (2015).
6. P. Del'Haye, A. Coillet, T. Fortier, K. Beha, D. C. Cole, K. Y. Yang, H. Lee, K. J. Vahala, S. B. Papp, and S. A. Diddams, Nat. Photonics **10**, 516 (2016).
7. T. Herr, V. Brasch, J. Jost, C. Wang, N. Kondratiev, M. Gorodetsky, and T. Kippenberg, Nat. Photonics **8**, 145 (2013).
8. V. Brasch, M. Geiselmann, T. Herr, G. Lihachev, M. Pfeiffer, M. Gorodetsky, and T. Kippenberg, Science **351**, 357 (2016).
9. X. Yi, Q.-F. Yang, K. Y. Yang, M.-G. Suh, and K. Vahala, Optica **2**, 1078 (2015).
10. P.-H. Wang, J. A. Jaramillo-Villegas, Y. Xuan, X. Xue, C. Bao, D. E. Leaird, M. Qi, and A. M. Weiner, Opt. Express **24**, 10890 (2016).
11. C. Joshi, J. K. Jang, K. Luke, X. Ji, S. A. Miller, A. Klenner, Y. Okawachi, M. Lipson, and A. L. Gaeta, Opt. Lett. **41**, 2565 (2016).
12. M. Karpov, H. Guo, A. Kordts, V. Brasch, M. H. Pfeiffer, M. Zervas, M. Geiselmann, and T. J. Kippenberg, Phys. Rev. Lett. **116**, 103902 (2016).
13. Q.-F. Yang, X. Yi, K. Y. Yang, and K. Vahala, Optica **3**, 1132 (2016).
14. C. Milián, A. V. Gorbach, M. Taki, A. V. Yulin, and D. V. Skryabin, Phys. Rev. A **92**, 033851 (2015).
15. P. Del'Haye, O. Arcizet, M. L. Gorodetsky, R. Holzwarth, and T. J. Kippenberg, Nat. Photonics **3**, 529 (2009).
16. X. Xue, Y. Xuan, C. Wang, P.-H. Wang, Y. Liu, B. Niu, D. E. Leaird, M. Qi, and A. M. Weiner, Opt. Express **24**, 687 (2016).
17. M. Haelterman, S. Trillo, and S. Wabnitz, Opt. Commun. **91**, 401 (1992).
18. S. Coen, H. G. Randle, T. Sylvestre, and M. Erkintalo, Opt. Lett. **38**, 37 (2013).
19. X. Xue, F. Leo, Y. Xuan, J. A. Jaramillo-Villegas, P.-H. Wang, D. E. Leaird, M. Erkintalo, M. Qi, and A. M. Weiner, "Second-harmonic assisted four-wave mixing in chip-based microresonator frequency comb generation," arXiv: 1607.02711 (2016).
20. J. Wahlstrand, J. Willits, T. Schibli, C. Menyuk, and S. Cundiff, Opt. Lett. **32**, 3426 (2007).
21. C. Bao, A. C. Funk, C. Yang, and S. T. Cundiff, Opt. Lett. **39**, 3266 (2014).
22. C. Bao, J. A. Jaramillo-Villegas, Y. Xuan, D. E. Leaird, M. Qi, and A. M. Weiner, Phys. Rev. Lett. **117**, 163901 (2016).
23. E. Lucas, J. D. Jost, and T. J. Kippenberg, "Study on the detuning-dependent properties of a temporal dissipative Kerr soliton in an optical microresonator," arXiv: 1609.02723 (2016).
24. X. Yi, Q.-F. Yang, K. Y. Yang, and K. Vahala, Opt. Lett. **41**, 3419 (2016).
25. C. Bao and C. Yang, Phys. Rev. A **92**, 053831 (2015).
26. K. Ikeda, R. E. Saperstein, N. Alic, and Y. Fainman, Opt. Express **16**, 12987 (2008).
27. J. Wang, Y. Xuan, A. M. Weiner, and M. Qi, in *Conference on Lasers and Electro-optics (CLEO)* (Optical Society of America, 2014), paper STh1M–8.
28. C. Bao, L. Zhang, L. C. Kimerling, J. Michel, and C. Yang, Opt. Express **23**, 18665 (2015).
29. Q. Lin, O. J. Painter, and G. P. Agrawal, Opt. Express **15**, 16604 (2007).
30. H. Haus and E. Ippen, Opt. Lett. **26**, 1654 (2001).
31. C. Bao, W. Chang, C. Yang, N. Akhmediev, and S. T. Cundiff, Phys. Rev. Lett. **115**, 253903 (2015).
32. H. Haus, IEEE J. Quantum Electron. **11**, 736 (1975).